

Simulation of the wave evolution and power capture of an oscillating wave surge converter

Daniela Benites-Munoz¹, Luofeng Huang¹, Enrico Anderlini¹, Jose Marín-López², Giles Thomas¹

¹Department of Mechanical Engineering, University College London, London, United Kingdom

²Facultad de Ingeniería Marítima y Ciencias del Mar, Escuela Superior Politécnica del Litoral, Guayaquil, Ecuador

ABSTRACT

For oscillating wave surge converters (OWSC) the incident wave field is changed due to the movement of the flap structure. A key component influencing this motion response is the Power Take-Off (PTO) system used. This paper examines the relationship between incident waves and the perturbed fluid field near the flap using the Computational Fluid Dynamics method by using Reynolds Averaged Navier-Stokes (RANS) equations. Further, it investigates the influence of a PTO system in the energy extracted from regular waves. Whilst this wave evolution is not significant in the effective power captured by a unit device, it is of great importance when performing in arrays as neighbouring devices may influence each other.

KEY WORDS: wave energy; power take-off; oscillating wave surge converters; power capture; wave pattern; Computational Fluid Dynamics; OpenFOAM.

INTRODUCTION

The Oscillating Wave Surge Converter (OWSC) is one of the most promising operating devices that use Wave Energy Conversion (WEC) technology in terms of its energy absorption capabilities and hydrodynamic performance (Babarit 2015). This device consists of a surface-piercing buoyant flap rotating around a hinge fixed to the sea bottom. The pitching motion of the WEC device combined with a hydraulic Power Take-Off (PTO), which connects the flap to its base, captures the energy from nearshore ocean surface waves (Cameron et al. 2010).

The OWSC operates usually at intermediate water depth where the energy is extracted from the surge motion of the waves (Dhanak and Xiros 2016). Under the action of these incident waves the flap oscillates back and forth (see Fig. 1). This oscillatory motion is dominated by the diffraction and the radiation effects of the incident wave acting on the device. Whilst the first is related to the solid body as an obstacle encountered by the fluid flow, the latter is identified with the oscillatory motion of the flap and consequent generation of secondary wave fields. Both effects will depend on the size of the flap and its oscillation (Henry et al. 2010).

In conjunction with the Queen's University Belfast (QUB), Aquamarine Power (AP) developed and deployed the full-scale prototype of an OWSC called Oyster at the EMEC (European Marine Energy Centre)

site in Orkney. During and after the designing stage of the Oyster, QUB in cooperation with AP, undertook extensive experimental and numerical studies. These studies focused mainly on understanding the hydrodynamic response of the OWSC in different wave environments as well as in increasing its performance.

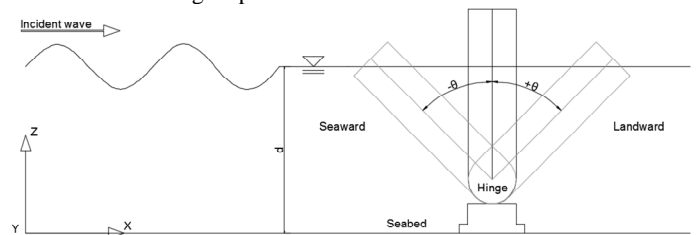


Fig. 1. Schematic two-dimensional drawing showing the motion of an oscillating wave surge converter under the action of the incident wave field.

Initial experimental studies regarding the response of a flap-type surface-piercing WEC to waves are reported in (Folley, Whittaker, and Henry 2007; Schmitt and Elsaesser 2015). These were early estimations of the power output and performance of the energy device under the action of small amplitude regular waves. Further two-dimensional experimental studies for OWSC were undertaken in order to understand the wave slamming phenomenon when the device operates in extreme sea conditions (Henry et al. 2014, 2015).

Using experimental models to understand the hydrodynamic performance of OWSC is generally demanding in terms of cost and time. To complement these experimental tests, numerical models are a viable alternative to estimate the performance of wave energy converters in the early stages of design. Various approaches of numerical modelling have been implemented to understand the hydrodynamic performance of OWSC with incident wave fields. These approaches include using the method based on potential flow theory (Renzi and Dias 2013; Renzi et al. 2014), smoothed particle hydrodynamics (SPH) method (Rafiee, Elsaesser, and Dias 2013; Brito et al. 2020), and the Computational Fluid Dynamics (CFD) method based on Reynolds averaged Navier-Stokes (RANS).

Among these methods, the CFD approach has been widely used, as it can account for more non-linear effects than the potential flow approach, whilst is much cheaper than experiments (Huang et al. 2019). Studies of the hydrodynamic response of OWSC to ocean waves have been carried

out by using the open-source software OpenFOAM and the commercial software FLUENT (Schmitt and Elsaesser 2015; Martínez-Ferrer et al. 2018; Wei et al. 2016). For the dynamic motion of the flap under the effect of the incident waves, these numerical models have used body fitted mesh for small angular displacements and arbitrary coupled mesh interface (ACMI) for large motions. In (Benites-Munoz, Huang, and Thomas 2019) the two-dimensional model of an OWSC performing under extreme sea conditions was studied using OpenFOAM software to solve the RANS equations combined with the overset mesh approach to handle the dynamic motion for large amplitudes.

A main element of a WEC is the Power Take-Off (PTO), which is used to transform the mechanical energy of the moving component into electrical energy. The PTO performance is crucial to assess the power obtained, and therefore is one of the first sub-systems included when analysing WEC devices (Windt, Davidson, and Ringwood 2018), and representing it in detail when performing numerical simulations is of current interest in the WEC industry (ITTC 2017). Due to the complex systems of the PTO associated to WEC devices, these are usually simplified using PTO force models by adding an external force back to the system (Brito et al. 2018).

Previous work considering the influence of the PTO in the operation of the OWSC includes the experimental work done by (Zhang et al. 2014; Brito et al. 2018) and the numerical and semi-analytical studies undertaken by (Brito et al. 2018, 2020; Behzad and Panahi 2017; Bacelli, Genest, and Ringwood 2015; Senol and Raessi 2019; Gomes et al. 2015). In these semi-analytical studies, the fluid problem set up using linear theory is solved by the application of numerical methods. To assess the power performance of WEC with the nonlinear PTO system, a high-fidelity CFD solution can be used (Windt, Davidson, and Ringwood 2018). The PTO has been represented as a rotational linear spring-damper or damper systems for surface-piercing OWSC numerically in (Gomes et al. 2015; Schmitt, Asmuth, and Elsaesser 2016; Brito et al. 2020).

In (Brito et al. 2020) an OWSC combined with a PTO was studied by SPH and validated against experimental tests. Moreover, the influence of the PTO damping characteristics and flap inertia in the power capture of the device was investigated. The range of the regular wave conditions of the 1:10 model include wave heights between 0.15 and 0.25 m and a wave period of 2.0 s (corresponding to a wavelength of 4.90 m). Furthermore, it was proved that the PTO system should not be neglected when analysing the hydrodynamics of OWSC for its influence on the Capture Width Ratio (CWR) of the device. The wave field, specifically the free surface elevation and the velocity distributions, is affected according to the damping coefficients used.

The first objective of this study is to understand the motion and wave energy extraction of the OWSC with a spring-damper system using the RANS method. Whilst the second aim is to use these results to analyse the wave pattern field around the WEC device operating under different wave conditions. To do this, an undamped OWSC (as shown in Fig. 1) is validated using OpenFOAM against experimental results. Following, the optimal damping coefficient, B_{opt} , at each wave frequency is calculated using the hydrodynamic coefficients for a flap-type pitching WEC in (Gomes et al. 2015). To complete the spring-damper system, the pitching stiffness coefficient, K , is taken for a vertical parallelepiped flap with uniform distributed mass. For each wave condition considered, the power capture factor, that is the percentage of energy available in the wave train absorbed by the PTO, is calculated. Further, the resulting wave field pattern around the device is analysed.

Following this introduction, this paper presents the employed numerical theories, the development of the CFD model, and their validations. Particularly, a practical approach to account for the PTO is introduced and the influence of the PTO on power capture analysed. The wave field around a single OWSC device is simulated and analysed, considering a range of different wave heights and periods based on the site of operation

of the full-scale prototype. Finally, the conclusion includes a brief summary and the implications of this study, as well as recommendations for further studies.

NUMERICAL APPROACH

The numerical model used for this study was first developed using a two-dimensional model (Benites-Munoz, Huang, and Thomas 2019), while here it is extended to be three-dimensional and further implemented with a PTO system. The simulation of the Numerical Wave Tank (NWT) with the flap-type WEC device is developed using the open-source software OpenFOAM. In the tank, two immiscible incompressible fluids, water and air are considered. The governing equations for this multiphase system include the continuity and momentum equations presented below:

$$\nabla \cdot \mathbf{U} = 0 \quad (1)$$

$$\frac{\partial \rho \mathbf{U}}{\partial t} + \nabla \cdot [\rho \mathbf{U} \mathbf{U}^T] = -\nabla p^* - \mathbf{g} \cdot \mathbf{x} \nabla \rho + \nabla \cdot [\mu \nabla \mathbf{U}] \quad (2)$$

\mathbf{U} and \mathbf{g} are the velocity and gravity vector fields, respectively. The density is ρ and p^* is the pseudo-dynamic pressure, $p = \rho \mathbf{g} \cdot \mathbf{x}$ (used as a numerical technique for the solution), \mathbf{x} is the position vector and μ is the dynamic viscosity. To estimate the solution of the governing equation the Finite Volume Method (FVM) is used, combined with the Volume of Fluid (VoF) approach, introduced in (Hirt and Nichols 1981), which is used to capture the interface between the air and the water.

The static boundary method combined with active wave absorption as detailed in (Higuera et al., 2013) is used for the generation of linear regular waves and absorption for the NWT. The most common wave conditions for power production are considered in the present study; therefore, highly nonlinear waves related to extreme conditions are not considered. Moreover, in this study, regular waves based on the operation site of the full-scale prototype, found in (O'Boyle et al. 2015), are used.

The mesh of the background domain is constructed with hexahedral cells, whilst the motion of the flap-type device is handled using the overset mesh, or chimera grid, technique. In this study, the cell sizes of the overset or front mesh are changed to match the size of the background mesh size, as this will decrease the interpolation error between the background and front meshes (Windt et al. 2019; Chan and Rogers 2002). The solution is achieved by the multiphase incompressible-fluid solver named *overInterDyMFOam* and the time-step is adjusted using the Courant Number (*CFL*). This number relates to the velocity flux crossing a grid cell in a given time-step. By using adjustable time discretisation, the time-step used is fixed according to the estimated value of the velocity in the cell, the size of the cell and the limit of *CFL*.

Throughout this work the OWSC device is assumed to be a rigid body with one degree of freedom (DOF), which is the pitching motion around the y-axis. The total force and moments come from the fluid and wave loads acting on the flap, the damping force exerted by the oscillatory motion of the flap and the restraint acting at the hinge at the bottom of the device. For the power capture calculations, it also includes an external moment applied to the hinge.

For the wave-structure interaction problem using overset grid approach, the RANS equations are first solved throughout the domain to estimate the fluid velocity and pressure distribution. Following that, to obtain the hydrodynamic force acting on the body located within the overset grid, the fluid pressure is integrated over the body's surface. Once the forces and moments that are acting on the body have been calculated, the translational and angular momentum equations of the rigid body are solved for its motion. Finally, the fluid and body properties and the overset mesh are updated, and the simulation continues with the iteration

for the next time step. The motion of the body is handled by the *sixDoFRigidBodyMotion* solver, available in OpenFOAM.

VALIDATION

The setup for the validation of the CFD model is based on the experimental test undertaken in QUB with a 1:40 scale model, whose particulars are retrieved from (Schmitt and Elsaesser 2015). The dimensions of the numerical tank are 20.0 x 1.8 x 0.6 m (length x width x height) and the water depth is 0.34 m. The dimensions of the flap-type energy converter model are 0.10 x 0.65 x 0.34 m (thickness x width x height) and rotates around the hinge located at 0.12 m from the bottom of the NWT (see schematic model in Fig. 2). The mass of the flap is 10.77 kg, its mass moment of inertia is 0.1750 kg·m² whilst the centre of gravity is at 0.12 m measured from the hinge. The flap-type model is located at 12.2 m from the wave-maker and waves generated are of height of 0.038 m and a period of 2.063 s, its wavelength corresponds to 4.208 m.

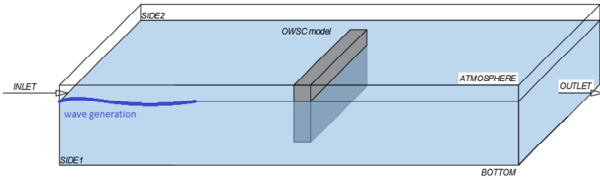


Fig. 2. Schematic of the numerical model, including the tank and the wave energy device.

The case was run in the UCL High-Performance Cluster (HPC) Grace, where the NWT is divided into 64-108 subdomains, depending on the number of cells considered, using the scotch decomposition method. By using this method, the programme balances the number of cells of each subdomain and its mesh complexity to be as close as possible to the other subdomains throughout the whole computational model (OpenFOAM ESI 2019). The solution of the fluid problem was done within each subdomain which is assigned to one processor, and later assembled for the post-processing analysis. This was done in order to perform the simulation more time-efficiently. The study case using 108 processors (or subdomains) takes 10 hours to run 40 s (or 20 wave periods) of simulation, with a time-step adjusted to a *CFL* of 0.65.

In numerical simulations the ideal aspect ratio (relationship between the length and the height of the cell) is 1. However, for numerical wave tanks, to maintain this ratio increases the computational cost considerably, specifically in regions where the accuracy of the solution or changes in the fluid/mesh are not significant. Because of this, the NWT have been refined in the areas of interest, namely the region close to the flap-type device and the free surface, R1 and R2, respectively, as seen in Fig. 3.

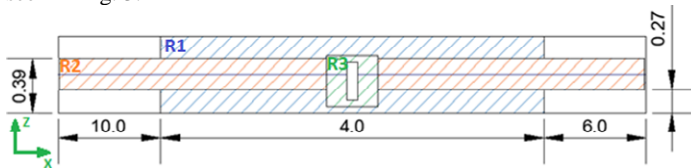


Fig. 3. Mesh refined regions in the model (Units: meters. Measures are not in scale. R1: region close to the device, R2: free surface region and R3: overset/front mesh).

For the analysis of the domain discretisation, the numerical simulations have been done considering 84, 140 and 210 cells per wavelength (λ) and 14, 20 and 30 cells per wave height (H_w), respectively. In each case the overset mesh (R3) was matched to the size of the background mesh. The width of the tank was discretised using cells of 0.05 m size (the same for the overset mesh in that direction).

The numerical results obtained of the rotation angles and angular velocity of the device performing under linear waves are presented in Fig. 4. In both graphics, the results obtained using 84 cells per wavelength are greater to those obtained with the refined cases. These last two cases seem to have reached the convergence, since between them, there is not significant relative difference between the rotation and angular velocity values.

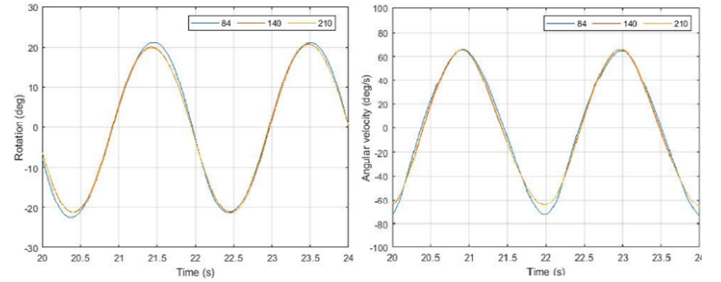


Fig. 4. Influence of varying mesh density, left: rotation angle, right: angular velocity.

The experimental test results of the 1:40 scale OWSC model, done at QUB (Schmitt and Elsaesser 2015), were used for the validation of the numerical model. These results included the tangential and radial accelerations, and these are compared to the numerical results undertaken in this study, as presented in Fig. 5.

The tangential acceleration is obtained by the equation $\mathbf{a}_t = \alpha_b r_t$, where \mathbf{a}_t is the tangential acceleration (m/s²), α_b is the angular acceleration (rad/s²) and r_t is the radius measured from the hinge location to the top of the plate. The equation for the radial acceleration is $\mathbf{a}_r = \omega^2 r$, where ω is the angular velocity (rad/s). However, for validation purposes, and in order to compare with the experimental tests \mathbf{a}_r is obtained from the equation $\mathbf{a}_r = \sqrt{\mathbf{a}_{tot}^2 - \mathbf{a}_t^2}$, where \mathbf{a}_{tot} is the total acceleration of the body in (m/s²) obtained using Newton's law $\mathbf{a}_{tot} = \frac{\mathbf{F}}{m}$ (\mathbf{F} is the total force and m is the mass of the body).

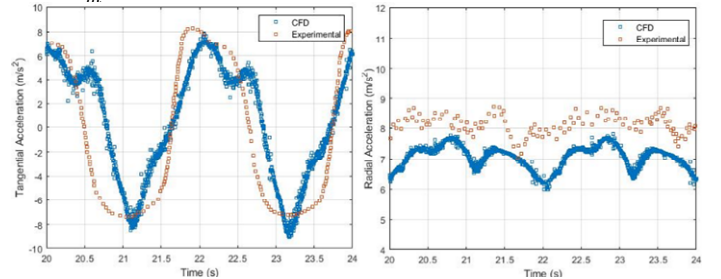


Fig. 5. Tangential (left) and radial (right) accelerations measured at the OWSC.

In both curves of the tangential and radial accelerations, the numerical result has a small shift from the experimental one, despite having similar trends. In the case of the tangential acceleration, there is sudden change in the positive values, which is not clearly appreciated in the experimental curve. Moreover, the values for the radial acceleration shown to have the same behaviour, but they have a relative difference of approximately 10%.

POWER CAPTURE

Study Cases

To assess the power capture of an OWSC, the sea conditions of the operating site of the Oyster are considered (O'Boyle et al. 2015). The 16 cases selected using different wave height and wave period are the most

frequent, and combined they represent 60% of the total occurrence of the sea states at the mentioned area. The wave parameters are scaled to a 1:40 model by using Froude scaling where the ratio for the wave height is equal to s (s is the scaling factor of 40) and for the period is $s^{0.5}$. The values already scaled and used in this study for regular waves are shown in Table 1.

Table 1. Wave parameters of the regular sea waves considered in the study.

Case	C01	C02	C03	C04	C05	C06	C07	C08
Height (m)	0.02	0.03	0.04	0.06	0.02	0.03	0.04	0.06
Period (s)	0.87	0.87	0.87	0.87	1.03	1.03	1.03	1.03
Case	C09	C10	C11	C12	C13	C14	C15	C16
Height (m)	0.02	0.03	0.04	0.06	0.02	0.03	0.04	0.06
Period (s)	1.19	1.19	1.19	1.19	1.34	1.34	1.34	1.34

Energy Extraction Calculation

If the modelling of the PTO is oversimplified, the power capture calculation of the WEC device could lead to overestimated values (Penalba et al. 2018). Thus, in this study the PTO is modelled using a spring-damper system (Gomes et al. 2015; Senol and Raessi 2019) in order to account for both the damping and the restoring forces. This system is added as a restraint in the motion of the OWSC as an external moment:

$$M_{PTO}(t) = B_m \dot{\theta}(t) - K\theta(t) \quad (3)$$

where B_m is the mechanical damping coefficient, K the pitch stiffness coefficient, θ is the flap motion amplitude and $\dot{\theta}$ the angular velocity. In this study, the system is matched to harness the maximum power capture for each wave condition considered. For this the damping coefficient is derived from linear theory and set to an optimum value for each wave frequency ω :

$$B_{opt} = \sqrt{B^2 + \left(\frac{C}{\omega} - \omega(I + A)\right)^2} \quad (4)$$

Where B is the radiation damping coefficient, C is the hydrostatic restoring coefficient, I is the moment of inertia and A is added moment of inertia. The hydrodynamic coefficients, B and A , are obtained from the curves given in (Gomes et al. 2015). The values of C and I are obtained for a simple plate assuming that its thickness is much smaller than its width and that the mass is uniformly distributed.

$$C = gtw h(\rho_w r_b - \rho_p r_c) \quad (5)$$

$$I = \frac{\rho_p t w d(t^2 + 4d^2)}{12} \quad (6)$$

where t , h and w are the thickness, height and width of the plate, respectively. The water depth is d . The densities of the plate and the seawater are identified with the variables ρ_p and ρ_w , whilst the centre of buoyancy and centre of the mass of the flap by the variables r_b and r_c . Whilst the optimum damping coefficient is varied for each wave period, the pitch stiffness coefficient is fixed to that of a vertical flap, as indicated by C .

Assuming the power is fully extracted by the PTO, the maximum absorbed power by the PTO is obtained with the following equation (Dhanak and Xiros 2016):

$$P = \frac{1}{2} \omega^2 B_{opt} |\theta_{max}|^2 \quad (7)$$

where θ_{max} is the maximum amplitude calculated from the numerical model. The estimation of the wave resource is defined as:

$$P_W = \frac{\rho_w g \omega H_w^2}{16k} \left(1 + \frac{2kd}{\sinh(2kd)}\right) \quad (8)$$

where k is the wave number.

The capture factor (C_f) is obtained from the ratio of the absorbed power and the available wave resource:

$$C_f = \frac{P}{P_W} \quad (9)$$

The unit of this ratio is meters and to nondimensionalise it, it is related to the characteristic length of the device, the width, by using C_f/w .

Power Take-Off System

Since this study is based on small-amplitude waves, the hydrodynamic coefficients calculated linearly in (Gomes et al. 2015) are used to estimate the optimal damping coefficient for each wave frequency. To obtain the added moment of inertia, A , and the radiation damping coefficient, B , the non-dimensional angular frequency is used, ω^* . This is obtained by the following equation:

$$\omega^* = \frac{\omega \sqrt{d}}{\sqrt{g}} \quad (10)$$

Finally, Table 2 shows the values of the optimal damping coefficients obtained.

Table 2. Optimal damping coefficients for each wave frequency of the study.

Cases	C01-04	C05-08	C09-12	C13-16
ω^*	1.35	1.16	0.97	0.87
B_{opt} (Nms/rad)	28.4	32.4	30.6	26.9

To verify the optimal value found for the damping coefficient, Case C16 is analysed for a range of B_m , including the calculated B_{opt} for that condition (26.9 Nms/rad) (see Fig. 6). This is done for two PTO systems, one only considering a damper (PTO_B) and the other considering a damper-spring system (PTO_B+K). It is worth noting that the B_{opt} does not give the highest absorbed ratio, denoted by C_f/w , and that can be due to the nonlinear viscous forces affecting the motion of the device. Another factor to bear in mind is that the assumption of small thickness compared to its width may not be applicable, suggesting additional nonlinear methods should be sought to calculate the hydrodynamic coefficients. Moreover, by adding the pitch stiffness constant, which in this case acts as a restoring force, it is expected to have an influence in the overall performance of the OWSC, specifically over the stability in the amplitude of the rotation (see Fig. 6). This variable is related to the tendency of the flap to right itself due to buoyancy.

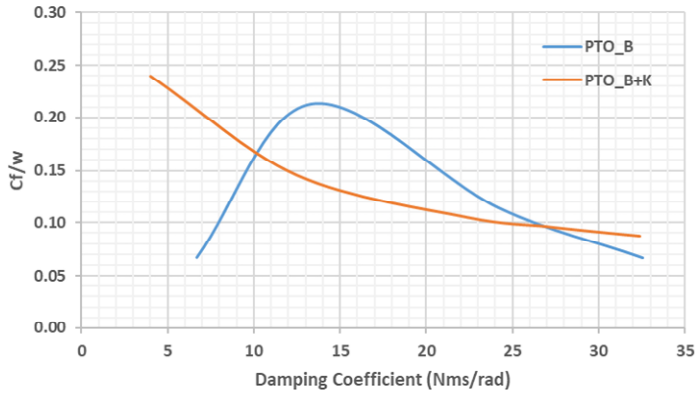


Fig. 6. Non-dimensional capture factor for different damping coefficients values applied to a spring-damper system in the power take-off.

Power Capture Estimation

In Fig. 7 it can be seen that for ω^* equal to 0.97 (corresponding in the model to $\omega = 5.21$ rad/s) the ratio of the power captured by the device is higher compared to other wave frequencies. In previous studies for undamped OWSC models it can be seen that when increasing the wave amplitude, the amplitude of the oscillation of the flap is higher. However, in the same figure (Fig. 7), it is shown that when considering the PTO, this is not a direct factor, but the combination of both, the wave frequency and its height.

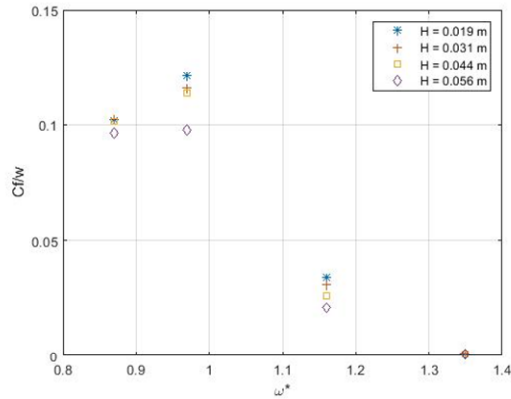


Fig. 7. Capture factor against the non-dimensional wave frequency for different wave heights.

In Fig. 8, the changes in the capture factor were compared using the wave height and frequency. It can be seen that despite increasing the wave height the variation in the capture factor appears to be minimum, compared to the effect of the variation of the wave frequency. To investigate this further, Fig. 9 presents the motion response of the flap against different wave heights, but for the same wave period of 1.19 s. The motion response is given by the ratio of the angle of rotation of the flap and the amplitude of the wave, A_w . It is noted that the influence of the pitch stiffness coefficient is high, since it acts in the direction contrary to the direction of the wave. However, it does not influence the maximum angle obtained from the motion of the OWSC.

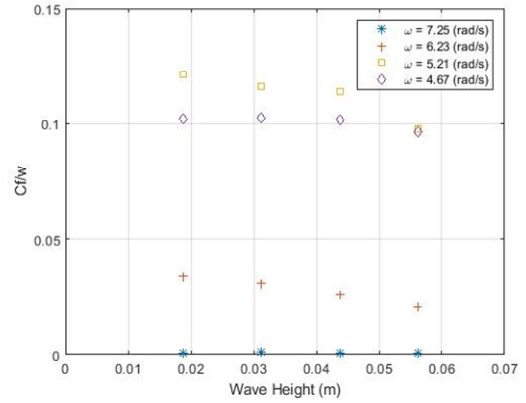


Fig. 8. Capture factor against the wave heights for different wave frequencies studied.

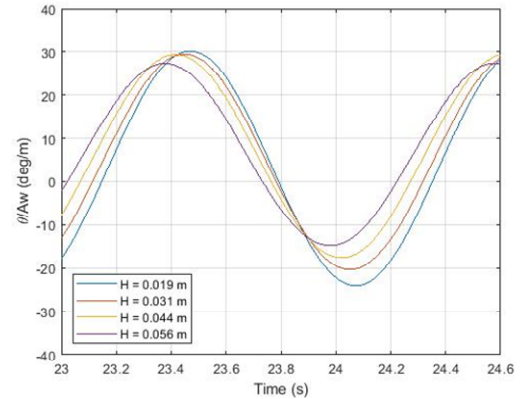


Fig. 9. Motion response per wave amplitude for Cases C09-C12.

WAVE PATTERN

According to Fig. 7-8, the case with the highest C_p/w is C09. In Fig. 10, the relative wave surface elevation in the NWT of this case is shown at three positions of the flap. The first is when the flap is at its maximum amplitude towards the land, the second at its upright position and the third at its maximum amplitude towards the sea (identified in the figure by (a), (b) and (c), respectively). In (a), the wave height towards the side of the flap is increased, as well as an additional wave radiated from the device. In the case of (b), when the wave field faces the upright flap as a fixed object, the diffracted wave shape can be appreciated on the sides by its change in the relative wave height. As in the case of (c), is similar to the case of (a), but the radiated wave is towards the sea, which will interact with the original generated wave.

This finding, while preliminary, suggests that this disturbance is not significant in the effective power capture of the OWSC operating as a single unit. However, it can imply that when considering devices operating in array configurations, it is of interest to understand the extent of the disturbed field. In this specific wave condition, it implies that the minimum location for a second device will be as its distance from the inlet (>12.20 m), which at scale will be approximately 500 m. Conversely, for the transverse direction, the NWT should require an extension in its width, to have a clearer appraisal of the behaviour of the diffracted waves.

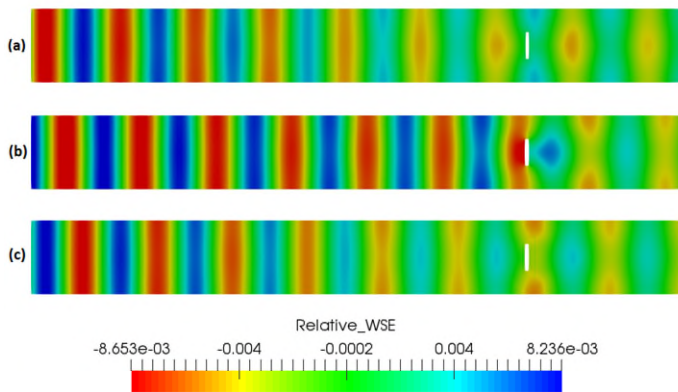


Fig. 10. Relative wave surface elevation when the flap is at three different positions: (a) Maximum oscillation (landwards), (b) Upright position and (c) Minimum oscillation (seawards).

CONCLUSIONS

Based on OpenFOAM, this study set out to determine the capture absorbed by the OWSC device combined with a PTO spring-damper system for different wave conditions of the site of operation of the full-scale prototype. To quantify an accurate damping will increase the power absorption whilst decreasing the amplitude of the oscillation of the flap. It was found that, with the PTO taken into consideration, the relationship of power capture is no longer positively correlated with the incident wavelength; instead, an optimal wave condition exists. Moreover, it is also found that the optimal damping coefficient calculated may be overestimated when is combined with the restoring force applied by the spring considered.

The efficiency of the energy extracted from the waves is related to high amplitude pitching motions of the device in short periods of time, as well as the capacity of the PTO to absorb the wave energy. Consequently, the incident wave field is disturbed due to the interaction with the flap and its motion. It is expected that the modified wave field caused by the motion of the OWSC becomes more relevant when it is performing in arrays with neighbouring devices.

ACKNOWLEDGEMENTS

The first author would like to acknowledge the financial support provided by the National Secretary of Higher Education, Science, Technology and Innovation (SENESCYT) and the Escuela Superior Politécnica del Litoral (ESPOL) of Ecuador.

REFERENCES

- Babarit, Aurélien. 2015. "A Database of Capture Width Ratio of Wave Energy Converters." *Renewable Energy* 80: 610–28. <https://doi.org/10.1016/j.renene.2015.02.049>.
- Bacelli, Giorgio, Romain Genest, and John V. Ringwood. 2015. "Nonlinear Control of Flap-Type Wave Energy Converter with a Non-Ideal Power Take-off System." *Annual Reviews in Control* 40: 116–26. <https://doi.org/10.1016/j.arcontrol.2015.09.006>.
- Behzad, Hamed, and Roozbeh Panahi. 2017. "Optimization of Bottom-Hinged Flap-Type Wave Energy Converter for a Specific Wave Rose." *Journal of Marine Science and Application* 16 (2): 159–65. <https://doi.org/10.1007/s11804-017-1405-y>.
- Benites-Munoz, Daniela, Luofeng Huang, and Giles Thomas. 2019. "The Interaction of Cnoidal Waves with Oscillating Wave Surge Converters." In *14th OpenFOAM Workshop*.
- Brito, Moises, R. B. Canelas, O. García-feal, J. M. Domínguez, A. J. C. Crespo, R. M. L. Ferreira, M. G. Neves, and L. Teixeira. 2020. "A Numerical Tool for Modelling Oscillating Wave Surge Converter with Nonlinear Mechanical Constraints." *Renewable Energy* 146: 2024–43. <https://doi.org/10.1016/j.renene.2019.08.034>.
- Brito, Moises, Luis Teixeira, Ricardo B. Canelas, Rui M. L. Ferreira, and Maria G. Neves. 2018. "Experimental and Numerical Studies of Dynamic Behaviors of a Hydraulic Power Take-Off Cylinder Using Spectral Representation Method" 140 (March): 1–13. <https://doi.org/10.1115/1.4037464>.
- Cameron, L., R. Doherty, Alan Henry, K. Doherty, J Van Hoff, D. Kaye, D. Naylor, S. Bourdier, and Trevor Whittaker. 2010. "Design of the Next Generation of the Oyster Wave Energy Converter." *3rd International Conference on Ocean Energy*, no. October: 1–12.
- Chan, William M, and Stuart E Rogers. 2002. "Best Practices in Overset Grid Generation." *Fluid Dynamics*.
- Dhanak, Manhar R., and Nikolaos I. Xiros. 2016. *Handbook of Ocean Engineering*. Springer. https://doi.org/10.1007/978-3-319-16649-0_5.
- Folley, M., T.J.T. Whittaker, and A. Henry. 2007. "The Effect of Water Depth on the Performance of a Small Surging Wave Energy Converter." *Ocean Engineering* 34 (8–9): 1265–74. <https://doi.org/10.1016/j.oceaneng.2006.05.015>.
- Gomes, R P F, M F P Lopes, J C C Henriques, L M C Gato, and A F O Falcão. 2015. "The Dynamics and Power Extraction of Bottom-Hinged Plate Wave Energy Converters in Regular and Irregular Waves." *Ocean Engineering* 96: 86–99. <https://doi.org/10.1016/j.oceaneng.2014.12.024>.
- Henry, Alan, Thomas Abadie, Jonathan Nicholson, Alan Mckinley, Olivier Kimmoun, and Frederic Dias. 2015. "The Vertical Distribution and Evolution of Slam Pressure on an Oscillating Wave Surge Converter," 1–11.
- Henry, Alan, Kenneth Doherty, Lisa Ann Cameron, Trevor Whittaker, and Rina Doherty. 2010. "Advances in the Design of the Oyster Wave Energy Converter." In *RINA Marine and Offshore Energy Conference*.
- Henry, Alan, Olivier Kimmoun, Jonathan Nicholson, Guillaume Dupont, Yanji Wei, and Frederic Dias. 2014. "A Two Dimensional Experimental Investigation of Slamming of an Oscillating Wave Surge Converter." *Proceedings of the International Offshore and Polar Engineering Conference*, no. January: 296–305. <http://www.scopus.com/inward/record.url?eid=2-s2.0-84906895131&partnerID=tZOtx3y1>.
- Hirt, C.W, and B.D Nichols. 1981. "Volume of Fluid (VOF) Method for the Dynamics of Free Boundaries." *Journal of Computational Physics* 39 (1): 201–25. [https://doi.org/10.1016/0021-9991\(81\)90145-5](https://doi.org/10.1016/0021-9991(81)90145-5).
- Huang, Luofeng, Kang Ren, Minghao Li, Željko Tuković, Philip Cardiff, and Giles Thomas. 2019. "Fluid-Structure Interaction of a Large Ice Sheet in Waves." *Ocean Engineering* 182: 102–11. <https://doi.org/10.1016/j.oceaneng.2019.04.015>.
- ITTC. 2017. "The Specialist Committee on Hydrodynamics Modelling of Marine Renewable Energy Devices." In *Proceedings of 28th ITTC - Volume II*.
- Martínez-Ferrer, Pedro J., Ling Qian, Zhihua Ma, Derek M. Causon, and Clive G. Mingham. 2018. "Improved Numerical Wave Generation for Modelling Ocean and Coastal Engineering Problems." *Ocean Engineering* 152 (September 2017): 257–72. <https://doi.org/10.1016/j.oceaneng.2018.01.052>.
- O'Boyle, Louise, Kenneth Doherty, Jos van 't Hoff, and Jessica Skelton. 2015. "The Value of Full Scale Prototype Data - Testing Oyster 800 at EMEC , Orkney." *Proceedings of the 11th*

- European Wave and Tidal Energy Conference*, no. September: 1–10.
- OpenFOAM ESI. 2019. “The Open Source CFD Toolbox.”
- Penalba, Markel, Josh Davidson, Christian Windt, and John V. Ringwood. 2018. “A High-Fidelity Wave-to-Wire Simulation Platform for Wave Energy Converters: Coupled Numerical Wave Tank and Power Take-off Models.” *Applied Energy* 226 (May): 655–69. <https://doi.org/10.1016/j.apenergy.2018.06.008>.
- Rafiee, Ashkan, Bjorn Elsaesser, and Frederic Dias. 2013. “Numerical Simulation of Wave Interaction With an Oscillating Wave Surge Converter.” *Ocean Engineering* 5.
- Renzi, Emiliano, and Frederic Dias. 2013. “Hydrodynamics of the Oscillating Wave Surge Converter in the Open Ocean.” *European Journal of Mechanics, B/Fluids* 41: 1–10. <https://doi.org/10.1016/j.euromechflu.2013.01.007>.
- Renzi, Emiliano, Kenneth Doherty, Alan Henry, and Frederic Dias. 2014. “How Does Oyster Work? The Simple Interpretation of Oyster Mathematics.” *European Journal of Mechanics, B/Fluids* 47 (June 2012): 124–31. <https://doi.org/10.1016/j.euromechflu.2014.03.007>.
- Schmitt, Pal, Henrik Asmuth, and Bjorn Elsaesser. 2016. “Optimising Power Take-off of an Oscillating Wave Surge Converter Using High Fidelity Numerical Simulations.” *International Journal of Marine Energy* 16: 196–208. <https://doi.org/10.1016/j.ijome.2016.07.006>.
- Schmitt, Pal, and Bjorn Elsaesser. 2015. “On the Use of OpenFOAM to Model Oscillating Wave Surge Converters.” *Ocean Engineering* 108: 98–104. <https://doi.org/10.1016/j.oceaneng.2015.07.055>.
- Senol, Koray, and Mehdi Raessi. 2019. “Enhancing Power Extraction in Bottom-Hinged Flap-Type Wave Energy Converters through Advanced Power Take-off Techniques.” *Ocean Engineering* 182 (March): 248–58. <https://doi.org/10.1016/j.oceaneng.2019.04.067>.
- Wei, Yanji, Thomas Abadie, Alan Henry, and Frédéric Dias. 2016. “Wave Interaction with an Oscillating Wave Surge Converter. Part II: Slamming.” *Ocean Engineering*.
- Windt, Christian, Josh Davidson, Dominic D.J. Chandar, and John V. Ringwood. 2019. “On the Importance of Advanced Mesh Motion Methods for WEC Experiments in CFD-Based Numerical Wave Tanks.” *VIII International Conference on Computational Methods in Marine Engineering MARINE 2019*, no. August: 145–56.
- Windt, Christian, Josh Davidson, and John V Ringwood. 2018. “High-Fidelity Numerical Modelling of Ocean Wave Energy Systems : A Review of Computational Fluid Dynamics-Based Numerical Wave Tanks.” *Renewable and Sustainable Energy Reviews* 93 (April): 610–30. <https://doi.org/10.1016/j.rser.2018.05.020>.
- Zhang, Da-hai, Wei Li, Hai-tao Zhao, Jing-wei Bao, and Yong-gang Lin. 2014. “Design of A Hydraulic Power Take-off System for the Wave Energy Device with An Inverse Pendulum *” 28 (2): 283–92. <https://doi.org/10.1007/s13344-014-0023-6>.